Extended Quantum Critical Phase in a Magnetized Spin-$\frac{1}{2}$ Antiferromagnetic Chain

M. B. Stone,[1,*] D. H. Reich,[1] C. Broholm,[1,2] K. Lefmann,[3] C. Rischel,[4] C. P. Landee,[5] and M. M. Turnbull[5]

[1]*Department of Physics and Astronomy, Johns Hopkins University, Baltimore, Maryland 21218, USA*
[2]*National Institute of Standards and Technology, Gaithersburg, Maryland 20899, USA*
[3]*Materials Research Department, Risø National Laboratory, DK-4000 Roskilde, Denmark*
[4]*Ørsted Laboratory, Niels Bohr Institute, University of Copenhagen, DK-2100, København Ø, Denmark*
[5]*Carlson School of Chemistry and Department of Physics, Clark University, Worcester, Massachusetts 01610, USA*

(Received 18 March 2003; published 17 July 2003)

Measurements are reported of the magnetic field dependence of excitations in the quantum critical state of the spin $S = 1/2$ linear chain Heisenberg antiferromagnet copper pyrazine dinitrate (CuPzN). The complete spectrum was measured at $k_BT/J \leq 0.025$ for $H = 0$ and $H = 8.7$ T, where the system is $\sim$30% magnetized. At $H = 0$, the results are in agreement with exact calculations of the dynamic spin correlation function for a two-spinon continuum. At $H = 8.7$ T, there are multiple overlapping continua with incommensurate soft modes. The boundaries of these continua confirm long-standing predictions, and the intensities are consistent with exact diagonalization and Bethe ansatz calculations.

DOI: 10.1103/PhysRevLett.91.037205 PACS numbers: 75.10.Jm, 75.40.Gb, 75.50.Ee

One of the most important ideas to emerge from studies of condensed matter systems in recent years is the concept of quantum criticality [1]. A quantum critical point marks a zero temperature phase transition between different ground states of a many-body system as a result of changes in parameters of the underlying Hamiltonian. Precisely at the quantum critical point, the system is without characteristic length scales or energy scales, with power-law spatial correlations and gapless excitations. Finite temperature properties close to quantum criticality are anomalous and reflect universal properties of the underlying quantum field theory.

While fine-tuning of a parameter in a system's Hamiltonian is generally required to achieve quantum criticality, it is inherent to the spin $S = 1/2$ linear chain Heisenberg antiferromagnet (LCHAFM). The spin dynamics of the LCHAFM have been studied in a number of materials [2–6], and the elementary excitations are $S = 1/2$ spinons that form a gapless, two-particle continuum [7,8]. In a magnetic field H, the Hamiltonian of the LCHAFM is $\mathcal{H} = \sum_i [J\mathbf{S}_i\mathbf{S}_{i+1} - g\mu_B H S_i^z]$. While changes in $\mathcal{H}$ such as the introduction of dimerization or interchain coupling drive the LCHAFM away from criticality [9], the system should remain quantum critical at $T = 0$ in fields below the fully spin polarized state, which occurs at $H_C = 2J/g\mu_B$ [10,11]. Prominent among the features predicted along this quantum critical line are a set of field-dependent two-particle continua [7,12–14] with incommensurate soft modes that move across the 1D Brillouin zone with H as $\tilde{q}_{i,1} = 2\pi m$ and $\tilde{q}_{i,2} = \pi - 2\pi m$, where $0 \leq m \leq 1/2$ is the magnetization per spin.

Experiments on copper benzoate [15] have verified the field dependence of $\tilde{q}_{i,2}$. However, due to a staggered g tensor and Dzyaloshinskii-Moriya interactions, the field drives that system away from the critical line to a state with confined spinons and a gap in the excitation spectrum [16]. In contrast, the finite-field critical state of the $S = 1/2$ LCHAFM is accessible in copper pyrazine dinitrate, $Cu(C_4H_4N_2)(NO_3)_2$ (CuPzN). This well characterized organometallic magnet has $J = 0.9$ meV, and negligible interchain coupling ($J'/J < 10^{-4}$) [6,17]. The spin chains in CuPzN have one Cu^{2+} ion per unit cell along the chain, and specific heat measurements have shown that CuPzN remains gapless for $H \leq 0.6H_C = 9$ T [6]. We report inelastic neutron scattering measurements of the spectrum of CuPzN at $H = 0$ and at $H = 8.7$ T, where $m = 0.15$. In zero field, the results are consistent with the exact two-spinon contribution to the spin fluctuation spectrum [8]. The high field data show the long-sought field-dependent continua [7], and are in detailed agreement with theoretical and numerical work [12–14].

Measurements were performed using the SPINS cold neutron triple axis spectrometer at the NIST Center for Neutron Research. The sample contained 22 single crystals of deuterated CuPzN with a total mass of 3.06 g, and a measured mosaic of 2° [18]. We used a dispersive analyzer configuration that detects scattered neutrons with an angular range of 10° and an energy range 2.7 meV $\leq E_f \leq$ 3.55 meV [19]. We used a Be filter before the sample for $E_i < 5.15$ meV, and a BeO filter after the sample. The elastic energy resolution was $\delta\hbar\omega = 0.14$ meV (FWHM), and the FWHM wave-vector resolution along the [100] chain axis was $\delta\mathbf{Q}_\parallel = 0.03$ Å^{-1} at $\mathbf{Q} = (hkl) = (\frac{3}{2}\frac{1}{4}0)$ at $\hbar\omega = 0$ [20]. Data were obtained between $\mathbf{Q} = (1\frac{1}{4}0)$ and $\mathbf{Q} = (2\frac{1}{4}0)$, with $H \parallel \hat{c}$.

Figure 1(a) shows the normalized magnetic scattering intensity $\tilde{I}_m(\tilde{q}, \omega)$ for CuPzN, at $H = 0$ and $T = 0.25$ K. Wave-vector transfer along the chain is represented as $\tilde{q} = 2\pi(h - 1)$. This data set was obtained by combining data taken at $E_i = 3.35$ meV, 3.55 meV, and for 3.75 meV $\leq E_i \leq$ 5.75 meV with 40 μeV steps. After subtracting the background scattering measured with

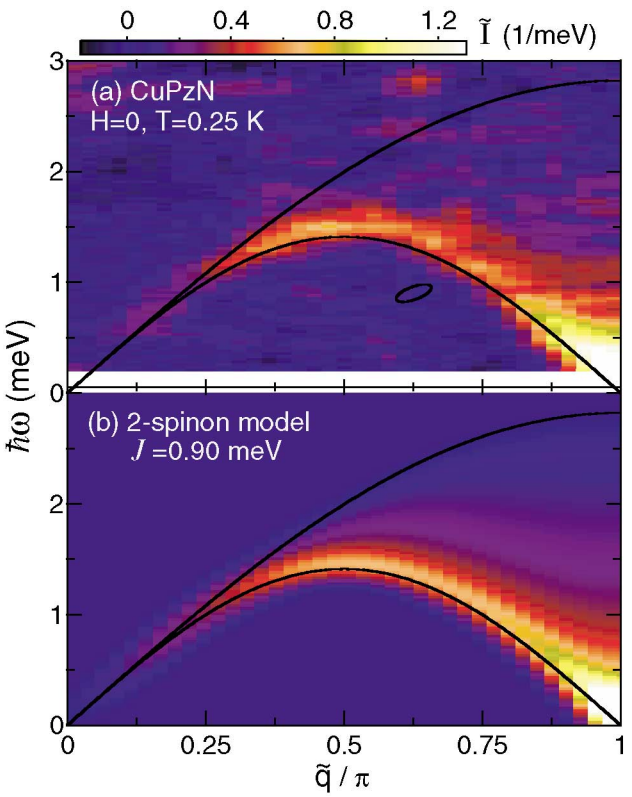

FIG. 1 (color). (a) Magnetic inelastic neutron scattering intensity $\tilde{I}_m(\tilde{q}, \omega)$ for CuPzN at $T = 0.25$ K and $H = 0$. (b) Calculated two-spinon contribution to $\tilde{I}_m$. Solid lines are the predicted lower and upper bounds of the spinon continuum. A representative FWHM resolution ellipsoid is shown in (a).

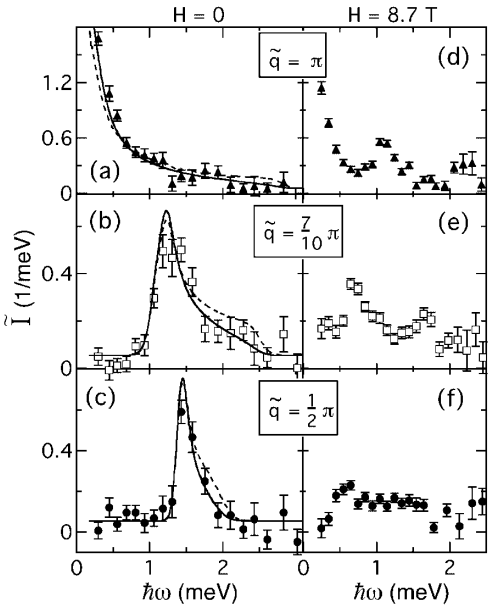

FIG. 2. Magnetic scattering intensity vs $\hbar\omega$ at constant $\tilde{q}$ for CuPzN at $T = 0.25$ K and $H = 0$ (a)–(c), and at $H = 8.7$ T (d)–(f). Each point includes scattering within a width of $\Delta\tilde{q} = 0.05\pi$. The solid (dashed) lines in (a)–(c) are the exact (approximate) theoretical results for $S(\tilde{q}, \omega)$ described in the text.

the analyzer in a nonreflecting geometry, the incoherent elastic scattering profile of the sample was determined from data that were at least 0.2 meV outside of the known bounds of the $H = 0$ spinon continuum (SC) for CuPzN [6]. This profile was scaled to the elastic incoherent scattering intensity at each $\tilde{q}$, and subtracted from the raw data. The data were converted to $\tilde{I}_m(\tilde{q}, \omega)$ by comparison with the incoherent scattering from vanadium. The data at $2\pi - \tilde{q}$ were then averaged with that at $\tilde{q}$, binned in bins of size $\delta\hbar\omega = 25$ μeV by $\delta\tilde{q} = 0.026\pi$, and averaged over a rectangle of the same size as the FWHM energy and wave-vector resolutions, yielding Fig. 1(a).

These data provide a complete picture of the zero-field SC in CuPzN. The solid lines are the SC bounds for $J = 0.9$ meV [7]. Figures 2(a)–2(c) and 3(a)–3(c) show cuts through the data, and highlight several important features. These include the monotonically decreasing intensity at $\tilde{q} = \pi$ [Fig. 2(a)], the peaks near $\tilde{q} = \pi$ associated with the divergence in $S(\tilde{q}, \omega)$ at the SC lower bound [8] [Figs. 3(a)–3(c)], and the smaller feature at low $\tilde{q}$ where the SC narrows as $\tilde{q} \to 0$ [Figs. 3(a) and 3(b)]. Figures 2(b) and 2(c) show the asymmetric line shapes produced by the SC for $\tilde{q} \neq \pi$. The intensity at $\tilde{q} = \pi$ decreases at $T = 35$ K [Fig. 3(c)], confirming that the scattering is magnetic.

Figure 1(b) shows $\tilde{I}_m(\tilde{q}, \omega)$ calculated [6] from the recently derived exact two-spinon contribution to $S(\tilde{q}, \omega)$ [8,21,22] with $J = 0.9$ meV, with the addition of a constant intensity fixed at the average residual background measured 0.5 meV away from the continuum. $\tilde{I}_m(\tilde{q}, \omega)$ is also shown as solid lines on the cuts in Figs. 2(a)–2(c) and 3(a)–3(c). There are no adjustable parameters in the model, and the agreement with the data is excellent, although we note that there is an overall 10% uncertainty in the vanadium normalization.

Figures 2 and 3 also show a comparison (dashed lines) to the line shapes produced by a fit to the approximate form [7] for $S(\tilde{q}, \omega)$ that has been previously used to model measurements of the $H = 0$ SC in CuPzN [6] and other materials [2,3]. This approximation is now known to overestimate $S(\tilde{q}, \omega)$ near the upper SC boundary [8,12]. Some indications of this are seen in Figs. 2(a)–2(c) and, although our data are not optimal for observing these differences, the exact two-spinon contribution to $S(\tilde{q}, \omega)$ provides a better description of the data.

The spectrum of CuPzN in a magnetic field is considerably more complex than at zero field, as seen in Fig. 4(a), which shows $\tilde{I}_m$ measured at $H = 8.7$ T. This data set combines data taken in the range 3.35 meV $\leq E_i \leq$ 4.75 meV with 20 μeV increments, and at $E_i = 5.15$ meV. An identical background subtraction, averaging, and binning procedure as used at $H = 0$ was applied to these data, using the $H = 0$ incoherent elastic profile.

Several new features emerge that were not present at $H = 0$. These are shown in the cuts in Figs. 2(d)–2(f) and

3(d)–3(f). A continuum is still seen at $\tilde{q} = \pi$ down to the lowest energy probed, which demonstrates that the system remains gapless and critical at $H = 8.7$ T. The spectrum has shifted to lower energy, and the strong ridge of scattering with linear dispersion near $\tilde{q} = \pi$ has a smaller slope showing explicitly that the velocity of the elementary excitations has decreased [6].

There is a strong peak in $\tilde{I}_m(\tilde{q}, \omega)$ centered at $\tilde{q} = \pi$ at the field energy $\hbar\omega = g\mu_B H \approx 1.1$ meV ($g_c = 2.07$ [23]). A weaker peak at this same energy can also be seen at $\tilde{q} = 0$, which corresponds to uniform spin precession. Moving away from $\tilde{q} = \pi$, there is another ridge of scattering intensity, which decreases in energy towards the expected field induced incommensurate wave vector $\tilde{q}_{i,2} = 0.7\pi$. As shown in Fig. 2(e), the incommensurate mode is seen in increased scattering at the lowest energies probed at $\tilde{q}_{i,2}$ compared to zero field [Fig. 2(b)]. Finally, a mode begins at the field energy at $\tilde{q} = 0$ decreases in energy with increasing $\tilde{q}$, and loses intensity close to $\tilde{q}_{i,1} = 0.3\pi$, consistent with numerical work [12].

Using the Bethe ansatz, Müller *et al.* identified six classes of excitations out of the partially magnetized ground state of an N-spin chain that can contribute to $S(\tilde{q}, \omega)$ [7]. Each class produces a continuum, and Müller *et al.* determined approximate expressions for the boundaries of these continua for $N \to \infty$. Three of these are predicted to dominate $S(\tilde{q}, \omega)$ for large N, with (adopting the notation of Ref. [7]) class (ii) contributing to $S_{zz}(\tilde{q}, \omega)$, class (iii) to $S_{-+}(\tilde{q}, \omega)$, and class (vi) to $S_{+-}(\tilde{q}, \omega)$. The boundaries of these three continua, $\mathcal{E}_2$, $\mathcal{E}_3$, and $\mathcal{E}_6$, are shown as solid lines in Fig. 4. They closely track the principal features of the data.

We have calculated $S(\tilde{q}, \omega)$ for chains of length $N = 24$, 26, and 28, using the Lanczos technique [12]. Figure 4(b) depicts the results for $N = 26$ and $m = 2/13$ ($H = 8.67$ T for CuPzN) [7]. Each eigenstate of the chain is marked by a circle with an area proportional to its contribution to $S(\tilde{q}, \omega)$ [12]. A circle's color indicates to which component of $S(\tilde{q}, \omega)$ the state contributes. Note that we measure $\mathcal{I}_m(\tilde{q}, \omega) \propto S_{zz} + \frac{1}{4}(S_{+-} + S_{-+})$.

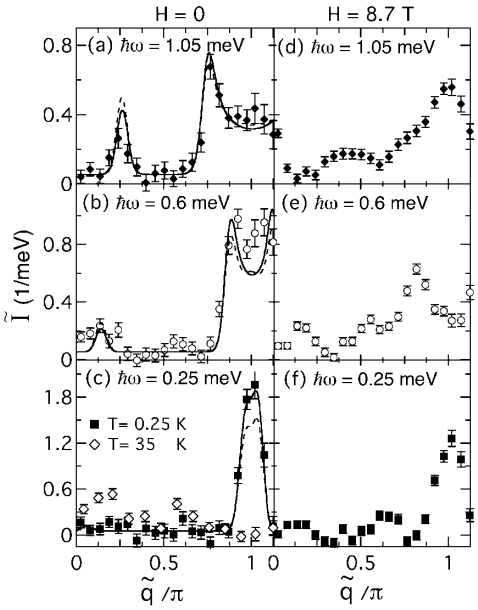

FIG. 3. Magnetic scattering intensity vs $\tilde{q}$ at constant $\hbar\omega$ for CuPzN at $T = 0.25$ K at $H = 0$ (a)–(c), and at $H = 8.7$ T (d)–(f). The data for $\tilde{q} < \pi$ have been averaged with the data at $2\pi - \tilde{q}$. The data displayed for $\tilde{q} > \pi$ have not been averaged. Each point includes scattering within a width of $\Delta\hbar\omega = 0.1$ meV. The solid (dashed) lines in (a)–(c) are the exact (approximate) theoretical results for $S(\tilde{q}, \omega)$ described in the text. Open symbols in (c): $T = 35$ K.

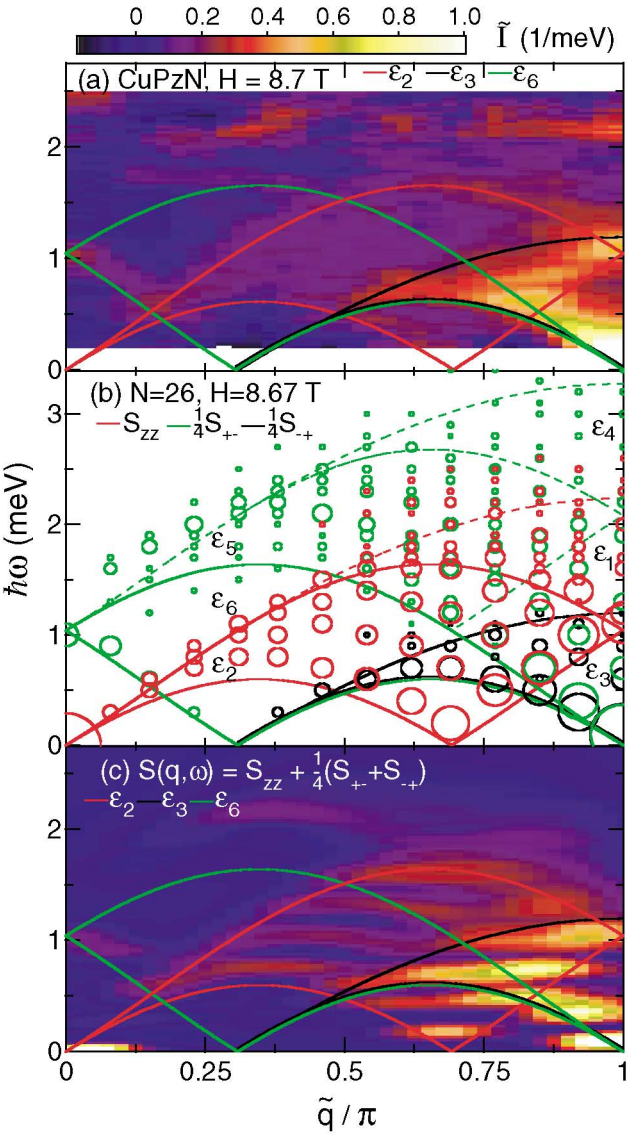

FIG. 4 (color). (a) Inelastic neutron scattering intensity $\tilde{\mathcal{I}}_m(\tilde{q}, \omega)$ for CuPzN at $T = 0.25$ K and $H = 8.7$ T. (b) Calculations of the different components of $S(\tilde{q}, \omega)$ for $N = 26$ spins and $m = 2/13$. The area of each circle is proportional to $S(\tilde{q}, \omega)$. (c) $\tilde{\mathcal{I}}_m(\tilde{q}, \omega)$ calculated for ensemble of chains with $N = 24$, 26, and 28. The curves in (a)–(c) show the bounds of the excitation continua $\mathcal{E}_1$–$\mathcal{E}_6$. Solid lines: Continua predicted to predominate as $N \to \infty$. In (b), $\mathcal{E}_2$(upper) = $\mathcal{E}_1$(lower).

The corresponding continuum boundaries are also color coded. Some spectral weight for this finite chain is seen outside of continua (ii), (iii), and (vi), and so for reference the boundaries of the other three continua, $\mathcal{E}_1$, $\mathcal{E}_4$, and $\mathcal{E}_5$, are included as dashed lines. The Lanczos technique gives accurate results for the excitation energies of finite-length spin chains [12], and although any finite-N calculation overestimates the energies of the infinite-N system, our results reproduce all trends and features of the data and, together with the continuum bounds, suggest polarization assignments.

A more direct comparison is achieved by combining the calculations in Fig. 4(b) with results for $N = 24$, $m = 1/6$, and $N = 28$, $m = 1/7$ ($H = 9.18$ T and 8.21 T for CuPzN), to increase the number of wave vectors sampled. The results at each N were convolved with the response function of a finite-size system, so that

$$S_{\alpha\beta}(\tilde{q}, \hbar\omega) = \sum_N \sum_{\tilde{q}_N} S_{\alpha\beta,N}(\tilde{q}_N, \hbar\omega) \left| \frac{\sin[(\tilde{q} - \tilde{q}_N)N/2]}{\sin[(\tilde{q} - \tilde{q}_N)/2]} \right|^2. \quad (1)$$

The calculated results were then converted to $\tilde{I}_m(\tilde{q}, \omega)$ [6], and binned and averaged as described above. After multiplication by an overall scale factor, we obtain Fig. 4(c) which is the scattering expected from an equal weighted ensemble of 24, 26, and 28 membered spin chains. While the relatively short chains yield stronger discrete energy bands than in the measurements, the simulation captures the main features of the data.

Karbach and Müller have recently identified a new type of quasiparticle for the three dominant classes of excitations, (ii), (iii), and (vi). These "psinons" play a similar role in the spectrum as do the spinons at $H = 0$, yielding a two-particle continuum for each component of $S(\tilde{q}, \omega)$ [13,14], with numerically determined boundaries that are consistent with the approximate ones shown in Fig. 4. Karbach *et al.* have computed the psinon line shapes for $m = 0.25$, where $\tilde{q}_{i,1} = \tilde{q}_{i,2} = \pi/2$ ($H = 11.9$ T for CuPzN), but a qualitative comparison to our data can still be made, as the line shapes should vary smoothly with H. Of particular interest is the peak predicted at the upper boundary of the psinon continuum for $S_{zz}(\tilde{q}, \omega)$, which is due to a singularity in the psinon density of states. This may explain the scattering intensity in Fig. 4(a) that tracks the top of the $\mathcal{E}_2$ continuum. This is notably different from the zero-field case, where the corresponding singularity in the spinon density of states is compensated by a vanishing matrix element, and $S(\tilde{q}, \omega)$ vanishes at the upper SC boundary, as seen in Fig. 1.

Finally, we note that Fig. 4(a) shows some evidence of weak scattering intensity for $\hbar\omega > 2$ meV. This could be due to the presence of short chains resulting from impurities, or to higher-order processes not included in the spinon/psinon picture. However, we note that our error bars are much larger here than at lower energy due to shorter counting times (see Fig. 2), and so a definitive statement on the existence of excitations in this energy range cannot be made at this time.

In summary, our experiments on CuPzN provide evidence for an extended critical state in a quantum magnet. The detailed mapping of the spin excitation spectrum in the spin-1/2 LCHAFM verifies long-standing predictions based on the Bethe ansatz of a field driven and critical incommensurate state. There is excellent agreement with finite chain calculations, and good qualitative agreement with the line shapes predicted at higher fields based on novel "psinon" quasiparticles. Recent advances in Bethe ansatz techniques show promise for full calculations of the psinons' contribution to $S(\tilde{q}, \omega)$ [14,24], and a direct comparison to our data would be very interesting.

This work was supported by NSF Grant No. DMR-0074571 and utilized facilities supported by NIST and the NSF under Agreement No. 9986442. X-ray characterization was carried out using facilities maintained by the JHU MRSEC under NSF Grant No. DMR-0080031.

*Currently at Department of Physics, The Pennsylvania State University, University Park, PA 16802, USA.

[1] S. Sachdev, *Quantum Phase Transitions* (Cambridge University Press, Cambridge, England, 2000).
[2] D. A. Tennant *et al.*, Phys. Rev. B **52**, 13 368 (1995).
[3] D. C. Dender *et al.*, Phys. Rev. B **53**, 2583 (1996).
[4] M. Takigawa *et al.*, Phys. Rev. B **56**, 13 681 (1997).
[5] M. Arai *et al.*, Phys. Rev. Lett. **77**, 3649 (1996).
[6] P. R. Hammar *et al.*, Phys. Rev. B **59**, 1008 (1999).
[7] G. Müller *et al.*, Phys. Rev. B **24**, 1429 (1981).
[8] M. Karbach *et al.*, Phys. Rev. B **55**, 12 510 (1997).
[9] R. Chitra and T. Giamarchi, Phys. Rev. B **55**, 5816 (1997).
[10] N. M. Bogoliubov *et al.*, Nucl. Phys. **B275**, 687 (1986).
[11] A. Fledderjohann *et al.*, Phys. Rev. B **54**, 7168 (1996).
[12] K. Lefmann and C. Rischel, Phys. Rev. B **54**, 6340 (1996).
[13] M. Karbach and G. Müller, Phys. Rev. B **62**, 14 871 (2000).
[14] M. Karbach *et al.*, Phys. Rev. B **66**, 054405 (2002).
[15] D. C. Dender *et al.*, Phys. Rev. Lett. **79**, 1750 (1997).
[16] I. Affleck and M. Oshikawa, Phys. Rev. B **60**, 1038 (1999).
[17] D. B. Losee *et al.*, J. Chem. Phys. **59**, 3600 (1973); G. Mennenga *et al.*, J. Magn. Magn. Mater. **44**, 89 (1984).
[18] M. B. Stone, Ph.D. thesis, Johns Hopkins University, 2002.
[19] I. Zaliznyak, J. Appl. Phys. **91**, 8390 (2002).
[20] N. D. Chesser and J. D. Axe, Acta Crystallogr., Sect. A **29**, 160 (1973).
[21] A. H. Bougourzi *et al.*, Phys. Rev. B **54**, R12 669 (1996).
[22] A. Fledderjohann *et al.*, Phys. Rev. B **53**, 11543 (1996).
[23] K. T. McGregor and S. G. Soos, J. Chem. Phys. **64**, 2506 (1976).
[24] D. Biegel *et al.*, Europhys. Lett. **59**, 882 (2002).